machines

MDPI

Article

Study on the Static Characteristics of a Pre-Pressure Single-Action Membrane-Type Restrictor Used in a Single Oil Pad

Feng Lu, Zhenzhong Wang *, Pengli Lei and Yi Chen

Department of Mechanical and Electrical Engineering, Xiamen University, Xiamen 361005, China; 19920191151156@stu.xmu.edu.cn (F.L.); kenash@mail.ustc.edu.cn (P.L.); 19920201151434@stu.xmu.edu.cn (Y.C.)
* Correspondence: wangzhenzhong@xmu.edu.cn

Abstract: In order to further improve the static stiffness of the hydrostatic bearing with the membrane-type restrictor, in this study, a static characteristics model of the pre-pressure single-action membrane-type restrictor (PSMR) is derived, and the criteria for achieving the optimum stiffness of the restrictor are summarized. A PSMR design method following the criteria of optimal stiffness is proposed. Then, the effect of design parameters on the performance of the restrictor is accurately evaluated by numerical simulation and orthogonal experiment with the grinder oil pad, as an example. Finally, the performance of the PSMR is compared with that of the traditional restrictors, and the main source of design error of the membrane-type restrictor is discussed. The results show that the effect of the design error of the membrane structure on the performance of the restrictor is reduced to some extent by the parallel oil circuit of the PSMR. In addition, the membrane-type restrictor designed according to the method of this paper theoretically has better static stiffness than the single-action membrane-type restrictor without pre-pressure, with an average improvement of about 14.14%.

Keywords: pre-pressure single-action membrane-type restrictor; theoretical modeling; numerical model; static characteristics

Citation: Lu, F.; Wang, Z.; Lei, P.; Chen, Y. Study on the Static Characteristics of a Pre-Pressure Single-Action Membrane-Type Restrictor Used in a Single Oil Pad. *Machines* **2022**, *10*, 302. https://doi.org/10.3390/machines10050302

Academic Editor: Angelos P. Markopoulos

Received: 17 March 2022
Accepted: 20 April 2022
Published: 24 April 2022

1. Introduction

The hydrostatic bearing has been widely used in precision machine tools due to its advantages: great load capacity, high motion accuracy, long service life, and excellent vibration absorption [1,2]. The membrane-type restrictor is a variable restrictor used on a hydrostatic bearing with a constant pressure oil source. Under the same external conditions, the performance of the hydrostatic bearing with the membrane-type restrictor is better than that of the hydrostatic bearing with the fixed-resistance-type restrictor whose flow resistance is constant, such as a capillary restrictor and a small hole restrictor [3,4]. In addition, its feedback element is a membrane, which has the characteristics of no sliding motion, no wear, a sensitive response, and an excellent dynamic performance [5]. Therefore, the membrane-type restrictor is the essential research object in the hydrostatic field.

Static characteristics of the hydrostatic bearing include static stiffness and load capacity, which are the most important indicators of hydrostatic bearings, significantly affecting the motion accuracy of the hydrostatic bearing. In recent years, scholars have investigated many studies on the static characteristics of the membrane-type restrictor. Academics have adopted a series of research methods to further improve the stiffness and load capacity of the hydrostatic bearing, such as mathematical modeling to analyze the performance of the membrane-type restrictor, using a combination of numerical simulations and experiments to modify the theoretical design equations, and optimizing the structure through numerical simulation, etc. Lai et al. [6,7] investigated the influence of the design parameters of the membrane-type restrictor on the static stiffness of the bearing and found that a reasonable dimensionless stiffness coefficient and design constraint ratio could theoretically achieve a high static stiffness of the open/closed bearing. Makoto Gohara et al. [8] demonstrated that the water-lubricated thrust bearing with membrane restrictor possessed an extremely

high static stiffness by numerical simulation and experiment. Chen et al. [9] used CFD software to investigate the performance of the membrane-type restrictor and proved the accuracy of the simulation model by experiment. Kang et al. have carried out extensive work on the membrane-type restrictor: regression analysis was carried out based on the experimental results to revise the equations of flow resistance and flow rate of the single-action membrane-type restrictor [10]; the numerical method was also used to evaluate the flow rate and flow resistance of the single-action membrane-type restrictor [11]; the design parameters of the single-action membrane-type restrictor and double-action membrane-type restrictor were optimized so that the static stiffness and load capacity of the bearings were theoretically optimal [12,13]. Zhu et al. [14] designed a new island-type membrane-type restrictor to avoid the deficiencies of the conventional membrane-type restrictors, in which the membrane was easy to warp and had much engineering design error.

Numerical simulation is a very efficient research method to analyze the static and dynamic characteristics of the restrictor and hydrostatic bearing. The Reynolds number is usually used by scholars to make inferences about the proper flow model for solving the fluid domain. The accuracy of the simulation model can be significantly reduced by an improper flow model due to the complexity of the flow. For example, the laminar flow may degenerate into turbulent flow when the bearing moves at high speed [15]; the vortex shedding phenomenon may be caused by obstructing structures of the oil cavity and the restrictor in the turbulent flow [16,17]. Hong et al. [18] studied the performance of the hydrostatic bearing under laminar flow and turbulent flow, respectively. It was shown that the simulation results of turbulent flow and laminar flow were similar at a small Reynolds number, and the turbulent flow model was more accurate at a large Reynolds number. Gohara et al. [8] and Hanawa et al. [19] investigated the static characteristics of the water-lubricated hydrostatic thrust bearing for the membrane-type restrictor and the capillary restrictor, respectively, using a laminar flow model. In particular, the water-lubricated hydrostatic thrust bearing was considered to work at low speed. Yuan et al. [20] investigated the static and dynamic characteristics of the hybrid water-lubricated bearing based on the turbulent Reynolds equations.

The Progressive Mengen (PM) flow controller is a pre-pressure single-action membrane-type restrictor developed and designed by Hyprostatik, Germany, with excellent restriction characteristics. Some scholars have studied its oil pressure regulation mechanism for engineering applications. Gao et al. [21], Chen et al. [22], and Dong et al. [23] investigated the application of PM flow controllers in hydrostatic guideways and analyzed the effect of PM flow controller regulation parameters on the dynamic and static performance of hydrostatic guideways, by methods such as mathematical modeling or genetic algorithms, to provide an effective theoretical direction for the selection of PM flow controller regulation parameters.

Inspired by the PM flow controller, the research group designed a pre-pressure single-action membrane-type restrictor (PSMR) based on the membrane-type restrictor described in the reference [10]. In this study, a static characteristics model is established based on the oil pressure regulation mechanism of PSMR. The effect of the design parameters on the static performance of the restrictor is analyzed by the model. Then, a design method of PSMR following the optimal stiffness criteria is proposed. The selection principles of the design parameters are optimized by the orthogonal experiment and numerical simulation. Finally, the static performance of the PSMR is compared with other types of restrictors by numerical simulation, the shortcomings of the design method of the membrane-type restrictor are analyzed, and the feasibility of this design method in engineering applications is discussed. It is shown that the static performance of the PSMR is better than that of the single-action membrane-type restrictor without pre-pressure (SMRWP).

2. Theoretical Modeling

In order to simplify the calculation, several assumptions should be made according to reference [1], as follows:

(1), The flow state of the fluid inside the hydrostatic bearing and the membrane-type restrictor is considered as laminar flow. (2), The fluid is assumed to be incompressible. (3), The inertia of the fluid is neglected. (4), The viscosity of the fluid is constant. (5), Only the membrane deformation is considered in the hydrostatic system, while everything else is rigid. (6), The external load points to the geometric center of the oil pad. (7), The flow rate of the inlet and outlet of the hydrostatic system is equal.

2.1. Pre-Pressure Single-Action Membrane-Type Restrictor

Housing, body, shim, and membrane are the key components of the PSMR. The restrictor's internal structure and the flow path of the oil are illustrated in Figure 1 [10,24]. The pump supplies oil with a pressure of P_s to the PSMR. The oil is divided into two streams as it enters the restrictor. One stream enters the regulating chamber through the small hole, which always ensures the oil pressure of the regulating chamber is P_s and plays the role of pre-pressure. With the other stream regulated by the annular rectangular groove, its pressure drops to P_t. Then, it is again divided into two streams, which form a special parallel oil circuit: one stream enters the oil cavity directly after being regulated by the annular capillary, and the other stream enters the pressure stabilizing chamber first and then flows into the oil cavity after being regulated by the annular cylindrical sill.

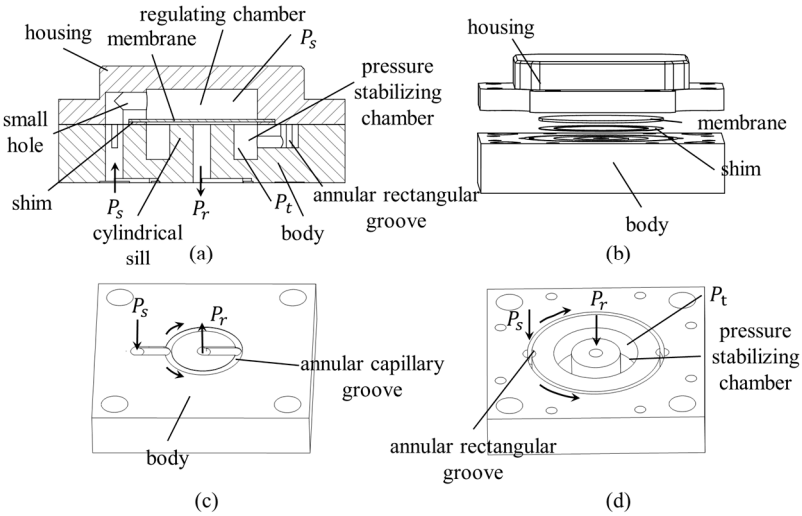

Figure 1. Structure of PSMR. (**a**) The sectional view of PSMR; (**b**) Parts of the PSMR; (**c**) Structure of the front side of the body; (**d**) Structure of the back of the body.

The single oil pad using a PSMR is shown in Figure 2, where r_{g1} is the inner radius of the cylindrical sill, r_{g2} is the outer radius of the cylindrical sill, and r_{g3} is the membrane radius. The PSMR works as follows [1,21,24]: at no load, the outlet pressure $P_r = 0$. Under the interaction of the regulating chamber pressure P_s, and the pressure stabilizing chamber pressure P_t, the membrane bends toward the cylindrical sill. At this time, the gap h_g between the membrane and the cylindrical sill is minimized, and the flow resistance of the PSMR is maximized. As the external load F increases (all of the calculations below assume that the external load F increases), P_r is raised and P_t is also changed. Then, the equilibrium state of the membrane is broken and the deflection of the membrane in bending is decreased, which makes an increase in h_g and a decrease in the flow resistance of the PSMR. The circuit analog for the oil pressure regulation of a single oil pad using a PSMR is shown in Figure 3.

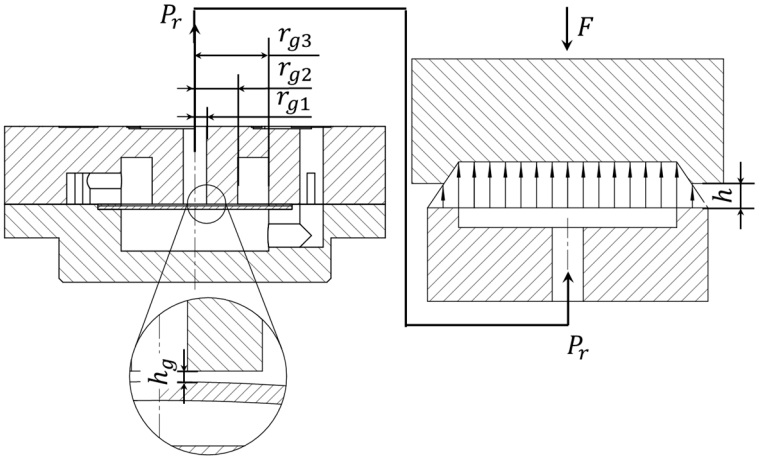

Figure 2. Single oil pad using a PSMR.

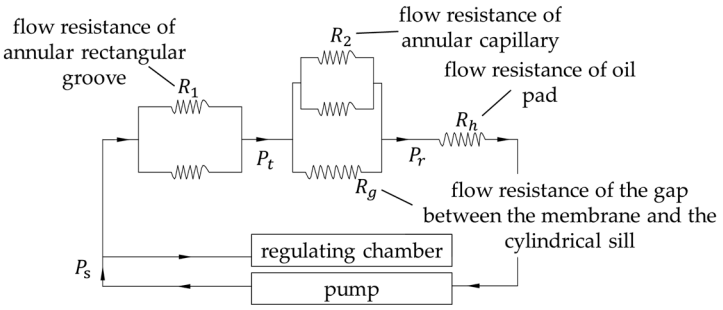

Figure 3. Analog circuit for a single oil pad using a PSMR.

2.2. Flow Rate Equation

Ohm's law of electrical circuits can be used to analyze the oil circuit [25]. When the external load is the initial load F_0, the hydrostatic bearing is in the initial state, the clearance of the oil pad h is h_0, and the gap h_g is h_{g0}. According to the flow continuity principle [1], the relationship between the pressure, flow rate and flow resistance of the PSMR can be derived:

$$\begin{aligned} R_{C0} &= \frac{R_2 R_{g0}}{R_2 + R_{g0}} \\ R_0 &= R_1 + \frac{R_2 R_{g0}}{R_2 + R_{g0}} + R_{h0} \\ Q_0 &= \frac{P_S}{R_0} = \frac{P_{t0} - P_{r0}}{R_{C0}} = \frac{P_{r0}}{R_{h0}} \end{aligned} \tag{1}$$

where: Q_0 is the inlet oil flow rate of the PSMR in the initial state; P_{t0} is P_t in the initial state; P_{r0} is P_r in the initial state; R_{C0} is the design flow resistance of the parallel oil circuit; R_0 is the design flow resistance of the restrictor; R_{h0} is the flow resistance of the clearance when the oil pad clearance is h_0; R_1 and R_2 are both fixed flow resistances of the annular groove, which are expressed in Equation (2); and when the gap between the membrane and the cylindrical sill is h_{g0}, R_{g0} is the flow resistance between the gap, which is expressed in Equation (3).

$$R_i = \frac{6\eta\pi r_i}{K_f b_i h_i^3} \tag{2}$$

$$R_g = \frac{6\eta \ln \frac{r_{g2}}{r_{g1}}}{\pi(h_{g0} - \Delta h_g)} = \frac{R_{g0}}{\left(1 - \frac{\Delta h_g}{h_{g0}}\right)^3} \tag{3}$$

where: η is the oil dynamic viscosity; r_i is the annular groove mid-diameter; b_i is the annular groove width; h_i is the annular groove depth; K_f is the groove flow coefficient; and Δh_g is

the increment corresponding to the gap h_g with increasing external load F. When $\Delta h_g = 0$, R_g is R_{g0}.

The clearance of the oil pad varies with the external load. It is assumed that the clearance h decreases as the external load F increases. The correlation between the flow resistance of the oil pad, R_h, and the oil pad clearance, h, is described by Equation (4):

$$R_h = \frac{R_{h0}}{(1 - A\varepsilon)^3} \tag{4}$$

where: A is the oil pad uneven coefficient, A = 1 for plane bearing, $A \neq 1$ for radial bearing; ε is the relative displacement of the geometric center of the oil pad, which satisfies $\varepsilon = \frac{e}{h_0}$, with e being the absolute displacement of the geometric center of the oil pad under the action of external load F. Combining Equations (1), (3) and (4), the flow rate expression for the non-initial state of the PSMR can be derived as follows:

$$Q = \frac{P_s}{R_1 + \frac{R_2 R_{g0}}{R_2\left(1 - \frac{\Delta h_g}{h_{g0}}\right)^3 + R_{g0}} + \frac{R_{h0}}{(1 - A\varepsilon)^3}} = \frac{P_t - P_r}{\frac{R_2 R_{g0}}{R_2\left(1 - \frac{\Delta h_g}{h_{g0}}\right)^3 + R_{g0}}} = \frac{P_r(1 - A\varepsilon)^3}{R_{h0}} \tag{5}$$

2.3. Load Capacity

The flow resistance ratios λ_1, λ_{21}, and λ_{22} in this study satisfy: $\lambda_1 = \frac{R_1}{R_h}$, $\lambda_{21} = \frac{R_2}{R_h}$, $\lambda_{22} = \frac{R_g}{R_h}$. Thus, in the design state, the design flow resistance ratios meet: $\lambda_{10} = \frac{R_1}{R_{h0}}$, $\lambda_{210} = \frac{R_2}{R_{h0}}$, $\lambda_{220} = \frac{R_{g0}}{R_{h0}}$. The restriction ratio β of the hydrostatic bearing system can be expressed as:

$$\beta = \lambda_1 + \frac{\lambda_{21}\lambda_{22}}{\lambda_{21} + \lambda_{22}} + 1 = \lambda_1 + \lambda_2 + 1 \tag{6}$$

where the resistance ratio $\lambda_2 = \frac{\lambda_{21}\lambda_{22}}{\lambda_{21} + \lambda_{22}}$. The design restriction ratio $\beta_0 = \lambda_{10} + \lambda_{20} + 1$, which is derived from Equation (6).

The load capacity w of a single oil pad can be described by Equation (7) [1]:

$$w = P_r A_e = \overline{F} P_s A_e \tag{7}$$

where A_e is the effective area of the oil pad and $\overline{F}$ is the dimensionless load factor of the hydrostatic bearing with values from 0 to 1. The mathematical expression of $\overline{F}$ can be derived from Equation (5).

$$\overline{F} = \frac{P_r}{P_s} = \frac{1}{1 + \lambda_{10}(1 - A\varepsilon)^3 + \frac{\lambda_{210}\lambda_{210}(1 - A\varepsilon)^3}{\lambda_{210}\left(1 - \frac{\Delta h_g}{h_{g0}}\right)^3 + \lambda_{220}}} = \frac{1}{\beta} \tag{8}$$

2.4. Membrane Deflection

Existing studies indicated that the fluid resistance of the membrane-type restrictor, calculated using the gap between the membrane and the cylindrical sill at r_{g1}, deviates the least from the experiment [26]. Figure 4 shows the approximate distribution of the oil pressure on the membrane inside PSMR [10]. The membrane deflection at r_{g1} is expressed by Equations (9)–(13) [10]. For the convenience of the calculation, K_1, K_2, and K_3 are used to represent the parts of Equations (9)–(13) that are directly related to the dimensions and material properties of the membrane.

$$\delta_A = \frac{12\left({r_{g3}}^2 - {r_{g1}}^2\right)^2 (1 - m^2)(P_s - P_t)}{64Et^3} = K_1(P_s - P_t) \tag{9}$$

$$\delta_B = \int_0^{r_{g1}} \frac{(P_t - P_r)r}{8D}\left[2(r^2 + {r_{g1}}^2)\ln(\frac{r_{g1}}{r_{g3}}) + \frac{(r^2 + {r_{g3}}^2)({r_{g3}}^2 - {r_{g1}}^2)}{{r_{g3}}^2}\right]dr = K_2(P_t - P_r) \tag{10}$$

$$\delta_C = \int_{r_{g1}}^{r_{g2}} \frac{((P_t - P_r) - \frac{(P_t - P_r)(r - r_{g1})}{r_{g2} - r_{g1}})r}{8D}\left[2(r^2 - {r_{g1}}^2)\ln(\frac{r}{r_{g3}}) + \frac{({r_{g1}}^2 + {r_{g3}}^2)({r_{g3}}^2 - r^2)}{{r_{g3}}^2}\right]dr = K_3(P_t - P_r) \tag{11}$$

$$D = \frac{Et^3}{12(1 - m^2)} \tag{12}$$

$$\delta = \delta_A + \delta_B + \delta_C = [(K_2 + K_3 - K_1)\lambda_2 + K_1\lambda]P_r \tag{13}$$

where: E is the elastic module; t is the membrane thickness; m is the Poisson's ratio.

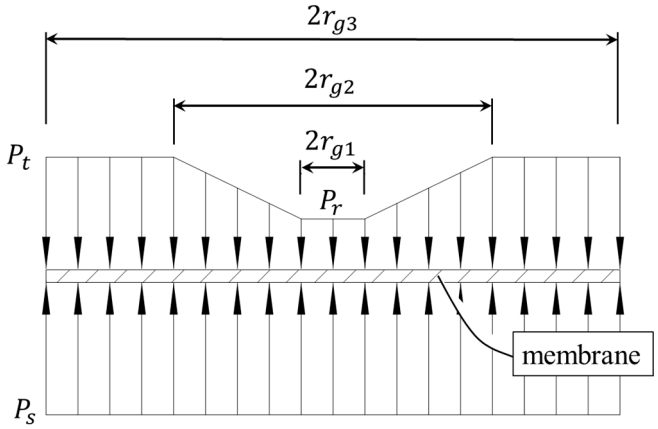

Figure 4. Pressure distribution on the membrane inside PSMR.

When the external load F increases, the pressure in the oil cavity would be also increased, and the corresponding increment can be noted as ΔP_r. For the membrane, Δh_g can be written as Equation (14), where $P_r = P_{r0} + \Delta P_r$

$$\Delta h_g = [(K_2 + K_3 - K_1)\lambda_2 + K_1\lambda]P_r - [(K_2 + K_3 - K_1)\lambda_{20} + K_1\lambda_0]P_{r0} \tag{14}$$

Expanding the expression (14) and omitting the higher-order terms of Δh_g, $A\varepsilon$, and ΔP_r, Δh_g can be written as:

$$\begin{gathered} \Delta h_g = m_1\Delta P_r - m_2 A\varepsilon \\ m_1 = \frac{(K_2+K_3-K_1)\lambda_{20}+K_1\lambda_0}{1-[(K_2+K_3-K_1)\lambda_{20}+K_1\lambda_0]\frac{3P_{r0}}{(1+\frac{\lambda_{220}}{\lambda_{20}})h_{g0}}} \\ m_2 = \frac{3[(K_2+K_3-K_1)\lambda_{20}+K_1\lambda_0]P_{r0}}{1-[(K_2+K_3-K_1)\lambda_{20}+K_1\lambda_0]\frac{3P_{r0}}{(1+\frac{\lambda_{220}}{\lambda_{20}})h_{g0}}} \end{gathered} \tag{15}$$

2.5. Static Stiffness in the Design State

Static stiffness is the load increment required for each unit of clearance change in the oil pad, and it is the most important indicator of the performance of the hydrostatic bearing. By Equation (5) it can be derived that:

$$Q = \frac{P_s - (P_{r0} + \Delta P_r)}{R_1 + R_g} = \frac{(P_{r0} + \Delta P_r)}{R_h} \tag{16}$$

Equation (16) can be written after expansion as:

$$\frac{P_s\left[1-(1-A\varepsilon)^3\right]}{R_{h0}\beta_0} = \Delta P_r\left[\frac{1}{R_g+R_1}+\frac{1}{R_h}-\frac{P_s}{\Delta P_r}\left(\frac{1-\frac{1}{\beta_0}}{R_g+R_1}-\frac{1-\frac{1}{\beta_0}}{R_{g0}+R_1}\right)\right] \tag{17}$$

Taylor series expansion for $\frac{1}{R_g+R_1}$:

$$\frac{1}{R_g+R_1} \approx \frac{1}{R_{g0}+R_1}+\left(\frac{1}{R_{g0}+R_1}\right)'\Delta h_g+\left(\frac{1}{R_{g0}+R_1}\right)''\Delta {h_g}^2 \tag{18}$$

Making use of Equations (15), (17) and (18) and omitting the higher-order terms of Δh_g, $A\varepsilon$, and ΔP_r, ΔP_r can be rewritten as:

$$\Delta P_r = \frac{\left[\frac{P_s(\beta_0-1)}{\beta_0}+\frac{3P_s{\lambda_{20}}^2 m_2 A\varepsilon}{h_{g0}\beta_0\lambda_{220}(\beta_0-1)}\right]}{\beta_0+\frac{3P_s{\lambda_{20}}^2 m_1}{h_{g0}\beta_0\lambda_{220}}} \tag{19}$$

Therefore, the static stiffness can be expressed as:

$$j_{u0} = -\left.\frac{\partial(\Delta P_r A_e)}{\partial h}\right|_{h=h_0} = -\frac{\left(\frac{3{\lambda_{20}}^2 m_2 A}{h_{g0}\beta_0\lambda_{220}(\beta_0-1)}\right)}{\beta_0+\frac{3P_s{\lambda_{20}}^2 m_1}{h_{g0}\beta_0\lambda_{220}}} * \frac{P_s A_e}{h_0} \tag{20}$$

The dimensionless stiffness coefficient is extracted from Equation (20):

$$\overline{j_{u0}} = -\frac{\left(\frac{3{\lambda_{20}}^2 m_2 A}{h_{g0}\beta_0\lambda_{220}(\beta_0-1)}\right)}{\beta_0+\frac{3P_s{\lambda_{20}}^2 m_1}{h_{g0}\beta_0\lambda_{220}}} \tag{21}$$

Clearly, the static stiffness of the hydrostatic bearing with the PSMR can theoretically reach infinity when it meets Equation (22) in the design state.

$$\frac{m_1 P_s}{h_{g0}} = \frac{-\lambda_{220}{\beta_0}^2}{3{\lambda_{20}}^2} \tag{22}$$

2.6. Static Characteristics Analysis

The infinite static stiffness of a hydrostatic bearing in the design state ($\varepsilon = 0$) does not mean that the relative displacement of the oil pad ε is at or near 0 when the hydrostatic bearing is in operation [1]. Therefore, this section investigates the effect of different design flow resistance ratios on the single oil pad using the PSMR, calculated by Matlab programming, using Equations (8) and (22). λ_{10}, λ_{210}, λ_{220} are the design parameters studied in this section.

As shown in Figure 5, the effect of $\overline{F}$ on ε is calculated in the single plane oil pad when four different combinations of parameters λ_{10} and λ_{220} are given, for different λ_{210}. Taking $\lambda_{10} = 0.001$ and $\lambda_{220} = 1$ as examples, when $\lambda_{210} = 0.5$, to keep $\varepsilon < 0.05$, the allowable range of $\overline{F}$ is 0.65~0.91; when $\lambda_{210} = 1$, the allowable range of $\overline{F}$ is 0.48~0.87. Clearly, when $\lambda_{210} < 1$, the clearance of the oil pad can only remain relatively constant over a narrow range of loads, regardless of the values taken for λ_{10}, λ_{220}. Inversely, when $\lambda_{210} > 1$, the clearance of the oil pad can be maintained near the initial value for a wide range of loads.

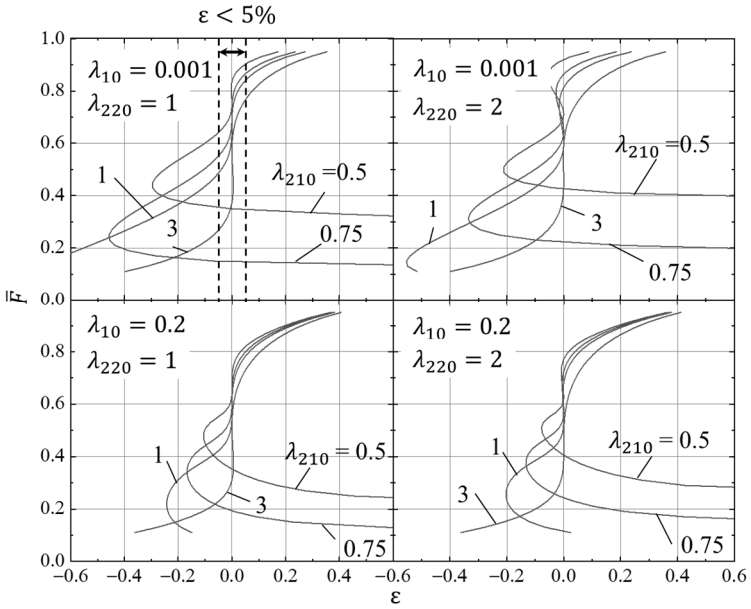

Figure 5. The effect of λ_{210} on the static characteristics of the oil pad.

The effect of $\overline{F}$ on ε in a single plane oil pad is calculated under different λ_{220} for four combinations of parameters λ_{10}, λ_{210}. Referring to Figure 6, the relative displacement of the oil pad ε can be maintained close to 0 for a wide range of loads when $\lambda_{220} > 0.5$. However, ε is so sensitive to $\overline{F}$ when $\lambda_{220} < 0.5$ that it cannot meet the demand.

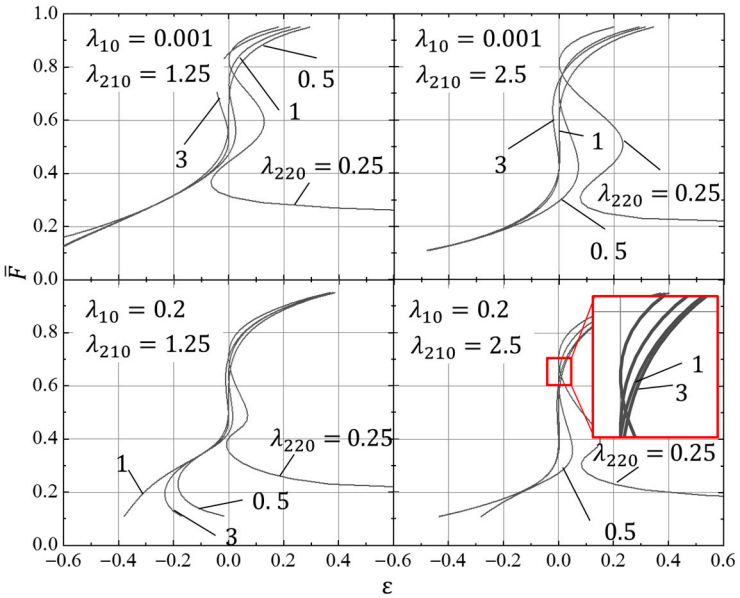

Figure 6. The effect of λ_{220} on the static characteristics of the oil pad.

Referring to the previous conclusion, the effect of $\overline{F}$ on ε is calculated for the single oil pad with a different flow resistance ratio λ_{10} for four combinations of parameters λ_{210}, λ_{220}. As shown in Figure 7, when λ_{210} and λ_{220} are properly designed, λ_{10} does not negatively affect the performance of the hydrostatic bearing in the range from 0 to 0.4.

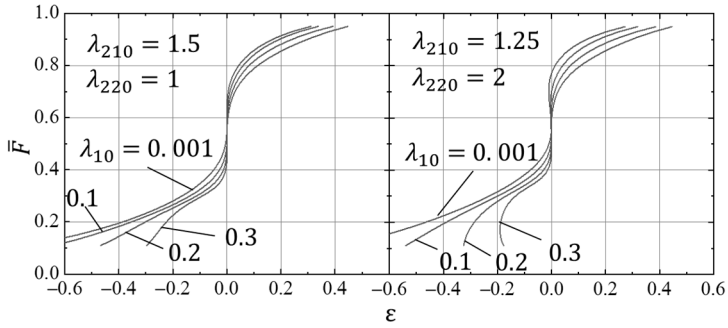

Figure 7. The effect of λ_{10} on the static characteristics of the oil pad.

Figures 5–7 reveal that the criteria for the infinite static stiffness of a single oil pad with the PSMR in the design state are sufficiently accurate. It can be concluded that the static characteristics of the hydrostatic bearing are excellent when $\lambda_{210} > 1$ and $\lambda_{220} > 0.5$ and Equation (22) is met. These are the criteria for the PSMR to achieve optimal stiffness.

3. Numerical Simulation

3.1. Numerical Model

In this section, a design method of the PSMR is proposed which follows the optimal stiffness criteria, referring to Figure 8. However, the optimal stiffness of the membrane-type restrictor cannot be achieved in practice due to the error in the engineering design [1]. The static stiffness of the membrane-type restrictor is only slightly better than that of the fixed-resistance-type restrictor [21]. In order to evaluate the static performance of the PSMR more accurately, the design method of the PSMR is adopted. Then, a two-way fluid-structure interaction (FSI) model is established using Ansys Fluent to simulate the static characteristics of the oil pad using the PSMR.

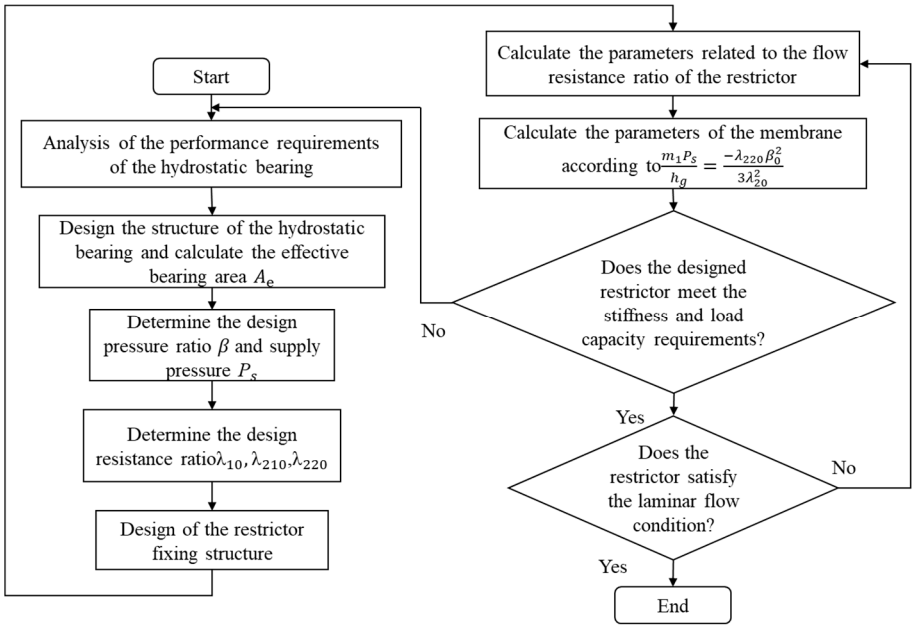

Figure 8. The design process of pre-pressure single-action membrane-type restrictor.

Referring to reference [2], the parameters of the hydrostatic guideway for a precision grinding machine are shown in Table 1, which adopts the rectangular oil pad. A VG 32 oil is used for the hydrostatic guide, whose dynamic viscosity η is 0.1214 Pa·s and density ρ is 960 kg/m^3.

Table 1. Parameters of the hydrostatic bearing system.

Parameters	Value	Parameters	Value
length of oil pad L/mm	200	width of oil sealing border a/mm	12
width of oil pad B/mm	75	h_0/mm	0.025
A_e/mm^2	11,844	P_s/MPa	3.2

The resistance of the rectangular oil pad is given by Equation (23). The initial flow resistance $R_{h0} = 2229$ Pa·s/mm^3 when $h_0 = 0.025$ mm.

$$R_h = \frac{6\eta a}{h^3((L-a)+(B-a))} \tag{23}$$

The FSI model of the PSMR is described in Figure 9. In the model, the high-order element and laminar flow model are adopted. Layering is adopted as the dynamic mesh method. The steady solver is adopted for the fluid domain model. The target for RMS change convergence of the FSI model for a two-way data exchange is 0.005. The number of fluid mesh layers in the annular rectangular groove, the annular capillary, and the gap between the membrane and the cylindrical sill is restricted to five or more layers. The skewness of the element is <0.9. 65 Mn is assigned as the material of the membrane, whose elastic modulus E = 210 GPa and Poisson's ratio m = 0.3. For the PSMR, r_{g1} = 1.5 mm r_{g2} = 5.5 mm, and r_{g3} = 9.5 mm. As shown in Equations (9)–(13), the membrane boundary condition in the theoretical model is often considered as a fixed constraint boundary instead of the frictional contact boundary in actual engineering, for the convenience of calculation [10]. In order to be consistent with the theoretical model, a fixed constraint boundary is adopted as the membrane boundary in the FSI model of this paper.

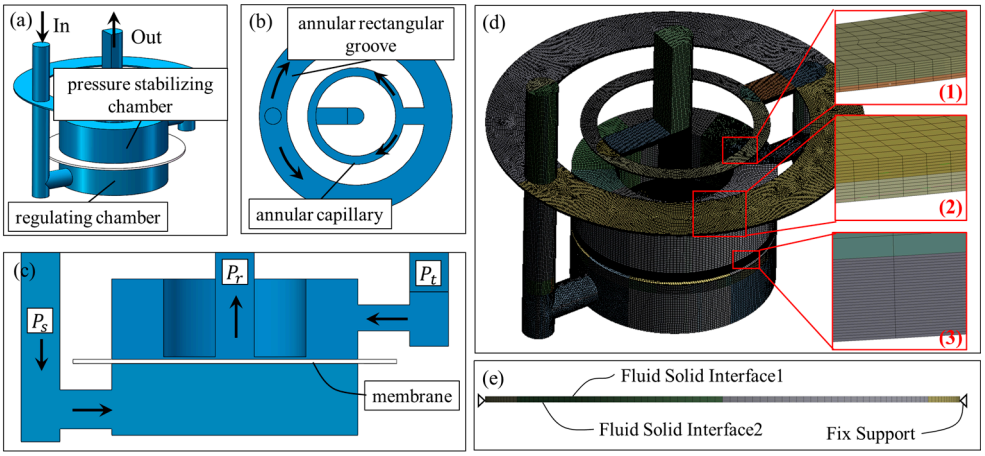

Figure 9. Geometric model and mesh model of PSMR. (**a**–**c**) the geometric model; (**d**) the mesh model of the fluid domain; (**e**) the mesh model of the membrane.

Numerical simulation is used to calculate the total flow resistance R and total flow rate Q of the restrictor for different P_r. Combined with the simulation results, the clearance h (assuming that the clearance of the oil pad is parallel under a different P_r) can be calculated by Equation (23), and the correlation curve between h and P_r is given. Since Equation (20) is available only in the design stage, the average static stiffness of the oil pad, j_{ua}, is calculated using the finite difference method.

$$j_{ua} = \frac{\Delta \overline{F} P_s A_e}{\Delta h} \tag{24}$$

3.2. Orthogonal Experiment

The design parameters λ_{10}, λ_{210}, and λ_{220} are designated as factors for the orthogonal experiment, and three levels are formulated for each experimental factor based on the results of the analysis in Section 2. The performance index of the orthogonal experiment is the average static stiffness of the oil pad in the outlet pressure range of P_{r0}~P_{r0} + 0.2 MPa. The factors and levels of the orthogonal experiment are given in Table 2.

Table 2. Factors and levels of the orthogonal experiment.

Levels	Factors		
	A	***B***	***C***
	λ_{10}	λ_{210}	λ_{220}
1	0.004	1.137	2.100
2	0.386	2.493	1.500
3	0.198	1.623	0.880

Table 3 is established by the orthogonal experiment table $L^9(3^4)$, with nine experiments planned. The calculated results related to the restrictor and the average static stiffness of the oil pad are listed in Table 3, where h_{ass} is the assembly gap of the membrane.

Table 3. Orthogonal experiment table.

No.	*A*	*B*	*C*	Blank Column	*t*/mm	h_{ass}/mm	j_{ua}/(N/μm)
1	1	1	1	1	0.3729	0.1081	1214
2	1	2	2	2	0.4406	0.0921	1453
3	1	3	3	3	0.4098	0.0979	1461
4	2	1	2	3	0.2681	0.3658	1941
5	2	2	3	1	0.3041	0.2738	1873
6	2	3	1	2	0.2897	0.3048	1807
7	3	1	3	2	0.3242	0.1881	1941
8	3	2	1	3	0.3761	0.1457	1743
9	3	3	2	1	0.3521	0.1623	1835
k_1	1376.0	1718.3	1588.0	1640.6			
k_2	1873.7	1689.7	1743.0	1753.3			
k_3	1859.3	1701.0	1778.0	1715.0			
Range	497.7	28.7	190.0	112.7			
Factor Priority				*A*, *C*, *B*			

It can be inferred from Table 3 that the average static stiffness of the restrictors with different design parameters has a great gap, even though all the restrictors are designed following the criteria of optimal stiffness. The j_{ua} of restrictors No. 7 and No. 4 is the best, 1941 N/μm, while the j_{ua} of restrictor No. 1 is the worst, only 1214 N/μm, with the former being 59.88% higher than the latter. Therefore, the selection principles of the design parameters of the PSMR require further optimization. The weights of the factors are revealed by the extreme differences. It can be concluded that λ_{10} has the strongest effect on the j_{ua} of the PSMR and λ_{210} has the weakest effect on the j_{ua} of the PSMR. From Figure 10, it can be observed that a larger λ_{10} with a smaller λ_{220} has a positive effect on the j_{ua} of the oil pad in the tested range. λ_{210} gives similar effectiveness as λ_{220}, but with a lower influence.

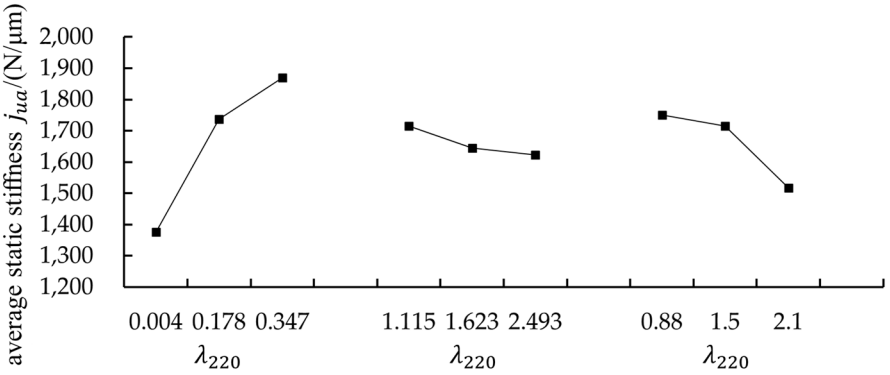

Figure 10. Trend diagram of orthogonal experiment.

3.3. Comparison of Static Characteristics of Three Types of Restrictors

In this section, the performance of the PSMR designed following the criteria of optimal stiffness is compared with that of traditional restrictors to investigate the feasibility of the proposed method in this paper for engineering applications. The capillary restrictor and the single-action membrane restrictor without pre-pressure (SMRWP) are assigned for comparison. Their design methods are adopted from reference [1]. The dimensions of the cylindrical sill of the SMRWP are the same as those of the PSMR. It is assumed that three working conditions are required for the hydrostatic system of the grinding machine, as follows: the initial dimensionless load factors of 0.56, 0.4, and 0.3, respectively; and the maximum dimensionless load factors of 0.71, 0.55, and 0.45, respectively. The initial dimensionless load factor is taken as the design dimensionless load factor, and the average static stiffness j_{ua} of the single oil pad over the load range is calculated, with all design parameters listed in Table 4.

Table 4. Table of design parameters.

No.	The Design Dimensionless Load Factor	Design Pressure Ratio						
		Capillary Restrictor	SMRWP	PSMR				
				λ_{10}	λ_{210}	λ_{220}	t/mm	h_{ass}/mm
1	0.66	1.7	1.7	0.198	1.137	0.88	0.3242	0.1881
2	0.5	2	2	0.228	1.623	1.30	0.3257	0.2094
3	0.4	2.5	2.5	0.374	5.476	1.40	0.3418	0.2109

The results are shown in Figure 11. The capillary restrictor has the lowest j_{ua}, and the average value of j_{ua} for the three capillary restrictors is only 1243 N/μm. The j_{ua} for the SMRWP designed following the optimal stiffness criterion is significantly better than that of the capillary restrictor, and the average value of j_{ua} for the three restrictors is 1570 N/μm, which is 26.31% higher than that of the capillary restrictor. The PSMR designed following the optimal stiffness criteria has the largest j_{ua} with an average value of j_{ua} of 1792 N/μm, which is 14.14% higher than that of the SMRWP.

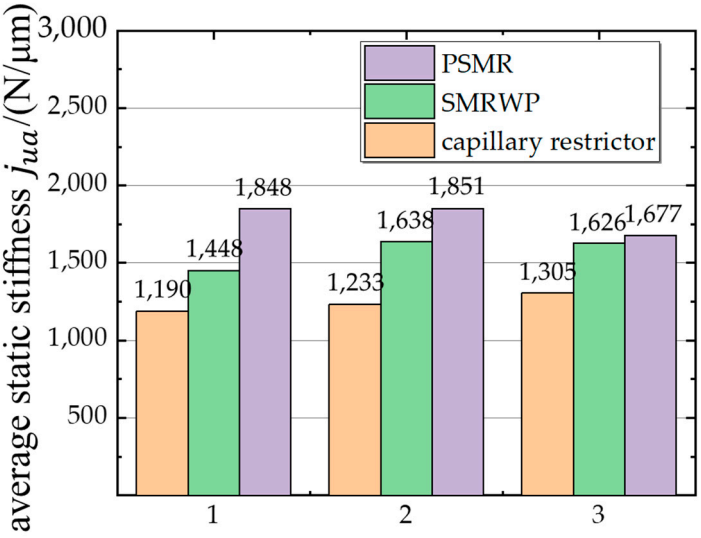

Figure 11. Simulation results of the average static stiffness of the three types of regulators.

3.4. Analysis and Discussion of the Membrane-Type Restrictor

In order to investigate the main reasons for the unsatisfactory design of the membrane-type restrictor, the simulated flow resistance of the restrictor is calculated by Equation (5) and analyzed by comparing it with the theoretical design values. The curves of the flow resistance for the three restrictors of No. 1 are plotted in Figure 12.

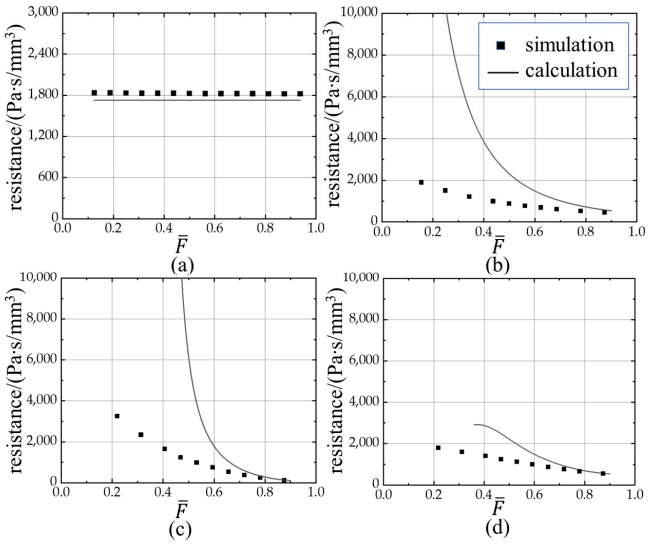

Figure 12. Simulation results of the flow resistance of the three types of restrictors. (**a**) Capillary restrictor; (**b**) single-action membrane restrictor without pre-pressure; (**c**) The gap between the membrane and the cylindrical sill for PSMR; (**d**) Pre-pressure single-action membrane-type restrictor.

It can be seen from Figure 12a that the flow resistance of the capillary restrictor is constant. In addition, the engineering design formula of the capillary restrictor is sufficiently accurate that the deviation of the flow resistance in the simulation from the theoretical calculation is less than 6%. Figure 12b reveals the characteristics of the SMRWP in that the flow resistance is an F-dependent variable. However, the calculation error of the flow resistance of the SMRWP is extremely great, which leads to its inability to achieve the optimal static stiffness in practical applications.

Figure 12c,d illustrate that the PSMR suffers from the same problem as the SMRWP, in that the flow resistance of the gap h_g obtained from the simulation deviates greatly from the theoretical calculation. However, in contrast to the enormous calculation error of R_g,

the simulated value of R for the PSMR deviates less from the theoretical calculation. This is mainly benefited by the parallel oil circuit, which is similar to the parallel circuit [27]. As shown in Equation (25), when the fixed flow resistance R_2 is calculated accurately enough, its error ξR_2 can be neglected, then the error ξR_C of the R_C is always smaller than the error ξR_g of the R_g. The R_2 obtained from the simulation is about 2338 Pa·s/mm^{3,} and that of the theoretical calculation is 2484 Pa·s/mm^3, and the relative error between them is only 6.24%, which means that the R_2 design is very accurate.

$$\zeta R_C = \frac{R_g}{R_g + R_2}\zeta R_2 + \frac{R_2}{R_g + R_2}\zeta R_g \tag{25}$$

It can be inferred from Figure 13 that there are two causes for the great deviation between the calculation and simulation of R_g. Firstly, as in Figure 13a, the pressure P_t obtained from the theoretical calculation is not accurate, but the theoretically calculated gap h_g has a good fit with the simulation, especially when $F > 0.5$, which instead indicates that the membrane deflection calculated in Equation (13) deviates significantly from the simulation. Secondly, as in Figure 13c, the gap between the membrane and the cylindrical sill is wedge-shaped instead of the parallel gap assumed in Equation (3), and the pressure distribution on the membrane is also different from the assumption, which causes the calculation of Equation (3) to be inaccurate as well.

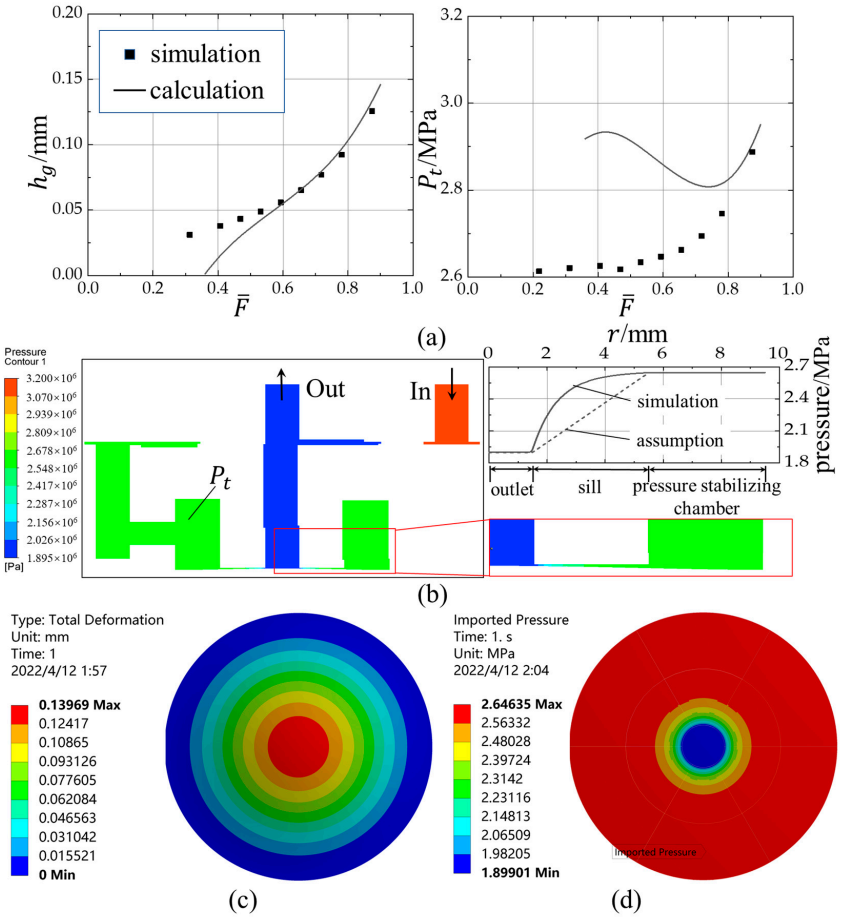

Figure 13. Simulation results and calculations of a PSMR for NO. 1. (**a**) Simulation results and calculations of PSMR; (**b**) Pressure field of PSMR when P_r = 1.9 MPa; (**c**) Deflection of the membrane toward the cylindrical sill when P_r = 1.9 MPa; (**d**) Pressure distribution on the membrane toward the cylindrical sill when P_r = 1.9 MPa.

4. Conclusions

In this paper, we analyze the performance of the PSMR using theoretical modeling and numerical simulation. The work and conclusions are summarized as follows:

(1) Based on the restriction theory of the PSMR, the theoretical model of the restrictor is established, and the criteria for achieving the theoretical best stiffness of the PSMR are obtained. The theoretical model shows that the theoretical performance of the PSMR is best when the design parameters of the restrictor satisfy $\lambda_{210} > 1$, $\lambda_{220} > 0.5$, and the criterion of infinite stiffness.

(2) In this paper, a PSMR design method that follows the optimal stiffness criteria is proposed. The performance of the PSMR designed based on this method is evaluated more accurately by the orthogonal experiment and the numerical simulation, and the principles for the selection of design parameters are optimized.

(3) The performance of the PSMR, SMRWP, and capillary restrictor under different working conditions is compared by numerical simulation. It is found that the PSMR designed by the method proposed in this paper has better static stiffness than the SMRWP in theory, with an improvement of about 14.14% for a single rectangular oil pad.

(4) Finally, this paper investigates the characteristics of fluid resistance of the capillary restrictor, SMRWP and PSMR in detail, introduces the pressure distribution and membrane deformation trend of the PSMR, and discusses the source of theoretical calculation error of membrane-type restrictors. The research results show that the error of the engineering design of the membrane-type restrictor mainly comes from the calculation of the flow resistance of the gap between the membrane and the cylindrical sill, while the parallel oil circuit structure of the PSMR reduces the calculation error of the total flow resistance of the restrictor to a certain extent.

Author Contributions: Conceptualization, F.L. and Z.W.; methodology, F.L. and P.L.; software, F.L. and P.L.; validation, F.L. and Z.W.; formal analysis, Z.W.; investigation, F.L.; resources, Y.C.; data curation, F.L.; writing—original draft preparation, F.L.; writing—review and editing, Z.W.; supervision, Z.W.; project administration, Z.W. All authors have read and agreed to the published version of the manuscript.

Funding: This research received no external funding.

Institutional Review Board Statement: Not applicable.

Informed Consent Statement: Not applicable.

Data Availability Statement: Not applicable.

Conflicts of Interest: The authors declare no conflict of interest.

Nomenclature

a	width of oil sealing border
A	unevenness coefficient of the pad
A_e	the effective area of the oil pad
b_i	width of annular rectangular groove or annular capillary
B	width of oil pad
e	absolute displacement of the geometric center of the pad
E	elastic module
F, F_0	external load, the initial load of hydrostatic bearing
$\overline{F}$	the dimensionless load factor
h	the clearance of the pad
h_g	the gap between membrane and cylindrical sill
h_0, h_{g0}	h and h_g in the initial state
Δh_g	increment of the gap between the membrane and cylindrical sill

h_i	depth of annular rectangular groove or annular capillary
h_{ass}	the assembly gap of the membrane
j_{ua}	the average static stiffness of the oil pad
K_f	flow coefficient of the rectangular groove
L	Length of oil pad
m	Poisson's ratio
m_1, m_2	membrane deformation coefficient
P_s	supply pressure, regulating chamber pressure
P_t	pressure stabilizing chamber pressure
P_r	the outlet pressure of restrictor
P_{r0}, P_{t0}	P_r and P_t in the initial state
ΔP_r	increment of outlet pressure
Q	the flow rate of restrictor
Q_0	Q in the initial state
r_i	mid-diameter of annular rectangular groove or annular capillary
r_{g1}, r_{g2}	inner radius, outer radius of restrictor sill
r_{g3}	radius of membrane
R_1, R_2	fixed flow resistance for annular rectangular groove, annular capillary
R, R_g, R_C	variable flow resistance of membrane restrictor, the gap between the membrane and the cylindrical sill, and the parallel oil circuit, respectively
R_h	flow resistance of the pad
R_0, R_{h0}, R_{g0}, R_{C0}	R, R_h, R_C and R_g in the initial state
ξR_2, ξR_C, ξR_g	the error of R_2, R_C, and R_g
t	membrane thickness
w	load capacity
β	restriction ratio
β_0	the design restriction ratio
δ, δ_A, δ_B, δ_C	membrane deflection at r_{g1}
ε	the relative displacement of the geometric center of the pad
η	oil dynamic viscosity
λ_1, λ_2, λ_{21}, λ_{22}	flow resistance ratio
λ_{10}, λ_{20}, λ_{210}, λ_{220}	the design flow resistance ratio
ρ	density

References

1. Ding, Z. *Fluid Hydrostatic Support Design*, 1st ed.; Shanghai Scientific and Technical Publisher: Shanghai, China, 1989; pp. 1–65.
2. Shi, C.; Wang, Z.; Peng, Y.; Lei, P.; Li, C. Quasi-static kinematics model for motion errors of closed hydrostatic guideways in ultra-precision machining. *Precis. Eng.* **2021**, *71*, 90–102. [CrossRef]
3. Moris, S.A. Passively and actively controlled externally pressurized oil-film bearing. *J. Lubr. Tech.* **1972**, *94*, 56–63. [CrossRef]
4. Sharma, S.C.; Sinhasan, R.; Jain, S.C. Performance characteristics of multiaccess hydrostatic/hybrid flexible journal bearing with membrane-type variable-flow restrictor as compensating elements. *Wear* **1992**, *152*, 279–300. [CrossRef]
5. PM-Regler-Fuer-Fuehrungen. Available online: https://hyprostatik.de/produkte-service/pm-regler-fuer-fuehrungen/ (accessed on 20 November 2021).
6. Lai, T.H.; Chang, T.Y.; Yang, Y.L.; Lin, S.C. Parameters design of a membrane-type restrictor with single-pad hydrostatic bearing to achieve high static stiffness. *Tribol. Int.* **2017**, *107*, 206–212. [CrossRef]
7. Lai, T.H.; Lin, S.C. A simulation study for the design of membrane restrictor in an opposed-pad hydrostatic bearing to achieve high static stiffness. *Lubricants* **2018**, *6*, 71. [CrossRef]
8. Gohara, M.; Somaya, K.; Miyatake, M.; Yoshimoto, S. Static characteristics of a water-lubricated hydrostatic thrust bearing using a membrane restrictor. *Tribol. Int.* **2014**, *75*, 111–116. [CrossRef]
9. Chen, D.C.; Chen, M.F.; Pan, C.H.; Pan, J.Y. Study of membrane restrictors in hydrostatic bearing. *Adv. Mech. Eng.* **2018**, *10*, 1–8. [CrossRef]
10. Kang, Y.; Shen, P.C.; Chang, Y.P.; Lee, H.H.; Chiang, C.P. Modified predictions of restriction coefficient and flow resistance for membrane-type restrictors in hydrostatic bearing by using regression. *Tribol. Int.* **2007**, *40*, 1369–1380. [CrossRef]

11. Kang, Y.; Shen, P.C.; Chen, C.H.; Chang, Y.P.; Lee, H.H. Modified determination of fluid resistance for membrane-type restrictors. *Ind. Lubr. Tribol.* **2007**, *59*, 123–131. [CrossRef]
12. Kang, Y.; Peng, D.X.; Hung, Y.H.; Hu, S.Y.; Lin, S.C. Design for static stiffness of hydrostatic bearings: Double-action variable compensation of membrane-type restrictors and self-compensation. *Ind. Lubr. Tribol.* **2014**, *66*, 322–334. [CrossRef]
13. Kang, Y.; Chen, C.; Chen, Y.; Chang, C.; Hsiao, S. Parameter identification for single-action membrane-type restrictors of hydrostatic bearings. *Ind. Lubr. Tribol.* **2012**, *64*, 39–53. [CrossRef]
14. Zhu, Y.H.; Liu, J.T.; Yang, J.X.; Bai, K. Design analysis of new structure of membrane restriction of liquid hydrostatic bearing. *Bearing* **2007**, *3*, 27–30.
15. Ram, N.; Sharma, S.C. Influence of wear on the performance of hole-entry hybrid misaligned journal bearing in turbulent regime. *Ind. Lubr. Tribol.* **2014**, *66*, 509–519. [CrossRef]
16. Cravero, C.; Marogna, N.; Marsano, D. A Numerical Study of correlation between recirculation length and shedding frequency in vortex shedding phenomena. *WSEAS Trans. Fluid Mech.* **2021**, *16*, 48–62. [CrossRef]
17. Shi, L.; Yang, G.; Yao, S. Large eddy simulation of flow past a square cylinder with rounded leading corners: A comparison of 2D and 3D approaches. *J. Mech. Sci. Technol.* **2018**, *32*, 2671–2680. [CrossRef]
18. Guo, H.; Xia, B.Q.; Cen, S.Q. Performance Analysis of High Speed Floating Ring Hybrid Bearing in the Laminar and Turbulent Regimes. *AMR* **2011**, *197–198*, 1776–1780. [CrossRef]
19. Hanawa, N.; Kuniyoshi, M.; Miyatake, M.; Shigeka, Y. Static characteristics of a water-lubricated hydrostatic thrust bearing with a porous land region and a capillary restrictor. *Precis. Eng.* **2017**, *50*, 293–307. [CrossRef]
20. Yuan, X.; Zhang, G.; Li, B.; Miao, X. Theoretical and experimental results of water-lubricated, high-speed, short-capillary-compensated hybrid journal bearings. In Proceedings of the International Joint Tribology Conference, San Antonio, TX, USA, 23–25 October 2006.
21. Gao, D.; Zhao, J.; Zhang, Z.; Zheng, D. Research on the Influence of PM Controller Parameters on the Performance of Hydrostatic Slide for NC Machine Tool. *J. Mech. Eng.* **2011**, *47*, 186–194. [CrossRef]
22. Chen, L.; Cui, B.; Zhao, J.; Gao, D. Influence of parameters of PM controller on vibration performance of liquid hydrostatic guide-way system. *Noise Vib. Worldw.* **2018**, *49*, 140–146. [CrossRef]
23. Dong, W.; Li, B.; Wu, C.; Zhou, Q.; Guo, W. Optimization Design Method for Hydrostatic Guideway Based on PM Restrictor. In Proceedings of the IOP Conference Series: Materials Science and Engineering, Chongqing, China, 18–21 July 2019.
24. Lin, T.Z. The Comparison of the Characteristcs for the New Type Design of Membrane Regulators. Master's Thesis, Chung Yuan Christian University, Taoyuan, Taiwan, July 2005.
25. Chen, Y. *Hydrostatic Bearing Principle and Design*, 1st ed.; National Defense Industry Press: Beijing, China, 1980; pp. 1–200.
26. Guangzhou Mechanical Engineering Research Institute Co., Ltd. *Principle and Application of Hydrostatic Bearing*, 1st ed.; China Machine Press: Beijing, China, 1978; pp. 1–85.
27. Lu, J. Error analysis of parallel resistance. *Meas. Tech.* **1981**, *7*, 43–44.